Photo-induced characteristics of TiO_2 prepared by anodic oxidation in sulfuric acid aqueous solution

Naoya Masahashi and Yoshiteru Mizukoshi

1. Background

TiO_2 oxide has been used as photocatalyst due to degrading toxic organic pollutants, bacteria, and viruses absorbed on its surface under ultraviolet (UV) light illumination [1-3]. The oxide is usually fabricated by wet (dip coating, spin coating, spraying) or dry (sputtering, ion-plating, vapor deposition) methods. Masahashi et al. studied an anodic oxidation to form photocatalyst TiO_2 on Ti and its alloys due to several advantages [4-8]. Firstly, it allows one to select the composition of electrolytes used for doping, which is beneficial for controlling the band gap structure of the oxide. Second, anodic oxidation occurs in equilibrium based on the thermodynamic reaction and provides adhesion strength at the interface. Third, it yields a porous microstructure due to the competitive reaction between oxide formation and chemical dissolution of the oxide by controlling the electrochemical parameters (conversion potential, current density and electrolyte composition), which influences the photocatalytic activities and superhydrophilicity. In our study, the primary concept is to develop crystallinity of anatase and/or rutile because it reduces a number of re-combination sites of photo-generated charges to promote photocatalytic reaction. The other is to control the electronic structure of the oxide by doping an element provided from the electrolyte improving visible light response of the oxide.

2. Experimental procedures

Substrate is a pure titanium plate used as the anode. Anodic oxidation was conducted in 0.002 M to 1.6 M sulfuric acid electrolyte using a Pt electrode for 0.5 h and was controlled galvanostatically until the conversion voltage reached a specified value. The anodic oxide was annealed at 723 K for 5 h in atmosphere. The crystallographic structure of the oxide was determined by X-ray diffraction (XRD) with Cu-K_α radiation with a thin-film geometry arrangement, and a rotating detector. Microstructure observations were conducted with field emission scanning electron microscopy and transmission electron microscopy (TEM). A TEM cross-sectional specimen was prepared by a focused ion beam. Surface roughness and surface area were measured using a laser microscope with a

wavelength of 408 nm. X-ray photoelectron spectroscopy (XPS) measurements were conducted with an electron spectrometer equipped with monochromated Al-K_α radiation.

The photocatalytic activity under UV light illumination was evaluated using methylene blue (MB) bleaching test and acetaldehyde decomposition test. The contact angle of distilled water (0.1 mL) is the average of three measurements taken for each sample by using a goniometer system. UV light of 0.1 mW/cm^2 intensity was radiated and the contact angle was measured every half hour during illumination.

3. Results

3.1. Microstructures

Figure1 shows micrographs of the anodic oxides in various concentrations of sulfuric acid [6]. When the sulfuric acid concentration is 0.02M, glassy anodized oxide with submicron sized pores is observed. The microstructure of the annealed oxide anodized in 0.1M sulfuric acid contains homogeneously distributed nanosized pores, followed by growth of the pores with an increase of the sulfuric acid concentration to 0.2M. Further increase of the sulfuric acid concentration to 1.2 M promotes unevenness of surface morphology and a coalescence of each pore appears frequently. The average pore size increases from approximately 170 to 950 nm with an increase in the concentration of sulfuric acid.

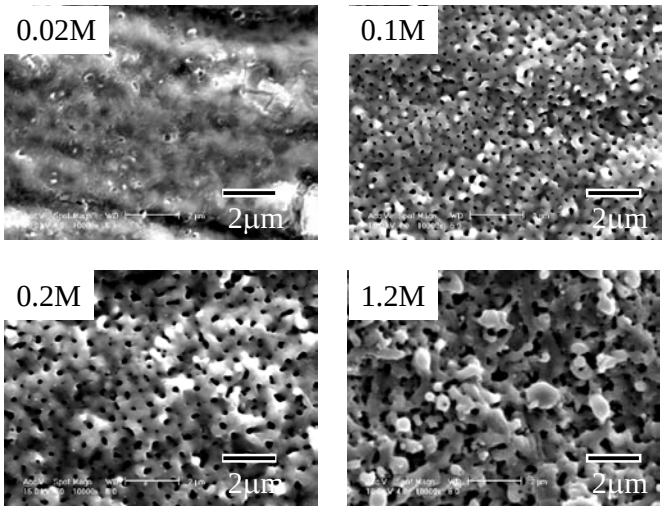

FIG.1 Micrographs of the anodic oxides in various concentrations of sulfuric acid of 0.02 M (a), 0.1 M (b), 0.2 M (c) and 1.2 M (d).

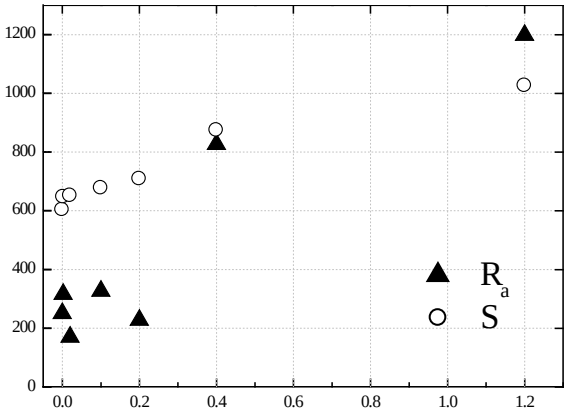

FIG.2 Plots of the surface area (S) and the average roughness (R_a) of the anodic oxide against the sulfuric acid concentration.

The surface area (S) and the average roughness (R_a) of the anodic oxide are plotted against the sulfuric acid concentration in the electrolyte (Fig. 2) [6]. It shows that both S and R_a increase with an increase of the sulfuric acid concentration in the electrolyte.

Figure 3 shows the cross-sectional TEM images of as-anodized (a) and annealed (b) oxides prepared in an electrolyte with a sulfuric acid concentration of 1.2 M [6]. It reveals that the thicknesses of the oxides are approximately 7 μm,

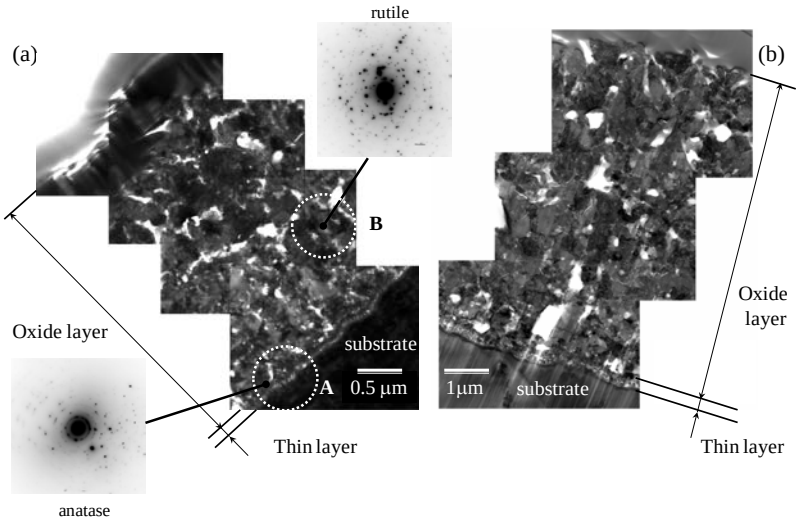

FIG. 3 Cross-sectional TEM micrographs of the as-anodized (a) and annealed (b) oxides anodized in an electrolyte with a sulfuric acid concentration of 1.2 M.

irrespective of annealing. A thin layer on the titanium substrate with a thickness of approximately 200 nm is observed in both the as-anodized and annealed oxides. The inserted bottom-left and top-middle diffraction patterns are obtained from the areas indicated by circles (A) and (B), respectively; the area circled (A) and circled (B) show the anatase and rutile form, respectively.

3.2 Crystal structure

Figure 4 is XRD profiles of as-anodized (left) and annealed (right) oxides prepared in an electrolyte with a sulfuric acid concentration of 0.02 M, 0.1 M, 0.2 M, 0.4 M, 1.2 M, and 1.6 M [6]. The peak intensity of the substrate hcp-Ti 101 (2θ = 40.18) decreases with an increase in the sulfuric acid concentration, indicating that the thickness of the oxide layer increases with the sulfuric acid concentration. The predominant oxide phase converted from anatase to rutile at 0.4 M of sulfuric acid. This implies that the rutile-structured phase is stabilized as the sulfuric acid concentration in the electrolyte is increased.

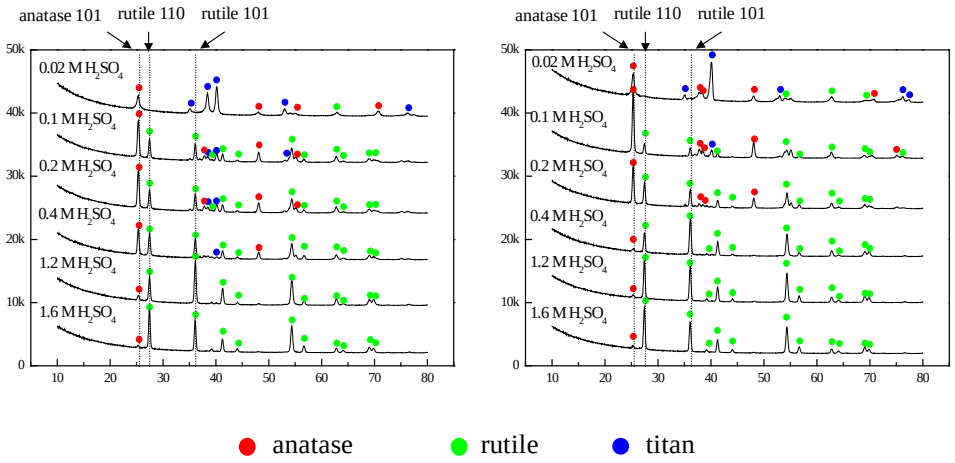

FIG.4 XRD profiles of the as-anodized (a) and annealed (b) oxides anodized in an electrolyte with a sulfuric acid concentration of 0.02 M, 0.1 M, 0.2 M, 0.4 M, 1.2 M and 1.6 M.

The crystallite size (ε) and inhomogeneous lattice strain (η) in the oxide were calculated from the full width at half maximum (FWHM) of the oxide peak by using Hall's methods. The parameters ε and η are plotted against the sulfuric acid concentration in the left and right of Figure 5, respectively [6]. In this figures, the parameters of the monolithic rutile TiO_2 powders with particle sizes of 1–2 μm was plotted to compare with those of the anodic oxide. The left figure shows

that the crystallite size varied between 10 nm and 30 nm and decreased slightly with annealing. The crystallite size of anatase increases with the sulfuric acid concentration in the electrolyte, irrespective of annealing, and the as-anodized oxide exhibits a larger crystallite size than that of the annealed oxide. However, the crystallite size of rutile is approximately 30 nm, irrespective of the sulfuric acid concentration, and no explicit difference is found between the as-anodized and annealed oxide. The right figure shows that the inhomogeneous lattice strain of the oxide is quite low or free (calculated as negative value) and annealing treatment further reduces the inhomogeneous strain. This implies that the amounts of lattice defects detectable by X-ray are so small, which is favorable to suppress recombination of the exited charges and improve photocatalytic activities.

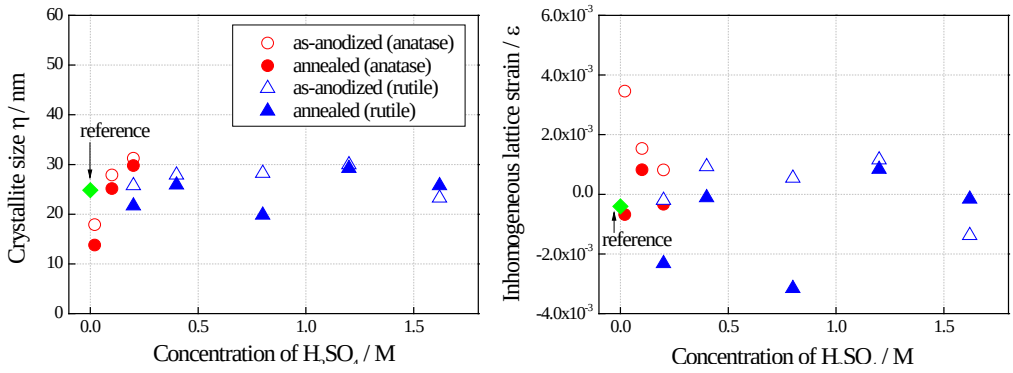

FIG.5 Crystallite size (a) and inhomogeneous lattice strain (b) of the as-anodized and annealed oxides versus the sulfuric acid concentration in the electrolyte.

3.3 XPS analysis

Figure 6 shows Ti 2p (left) and O 1s (right) XPS of the annealed oxides anodized in the electrolytes of a sulfuric acid concentration of 0.1 M and 1.2 M, respectively [6]. Two single peaks at approximately 465 eV and 459 eV correspond to the Ti^{4+} $2p_{1/2}$ and $2p_{3/2}$ contributions of TiO_2. The Ti 2p XPS reveals that the surface is completely composed of TiO_2. They have a symmetrical shape, indicating that reduced Ti^{3+} ions are not present in the oxides. It is beneficial for the photocatalysis to lower the recombination frequencies, because the reduced Ti^{3+} ions act as recombination sites. The O 1 s XPS profiles have an asymmetrical shape accompanied with a shoulder band at approximately 532.4 eV on the higher binding energy side of the main peak. This shoulder peak has been observed in the previous study and is ascribed to

hydroxyl groups [9]. It should be noted that the intensity of the shoulder peak in the oxide anodized in the electrolyte with a sulfuric acid concentration of 1.2 M is higher than that in the electrolyte of a sulfuric acid concentration of 0.1 M. This suggests that the former anodic oxide could adsorb a large amount of water molecule as compared to the latter oxide.

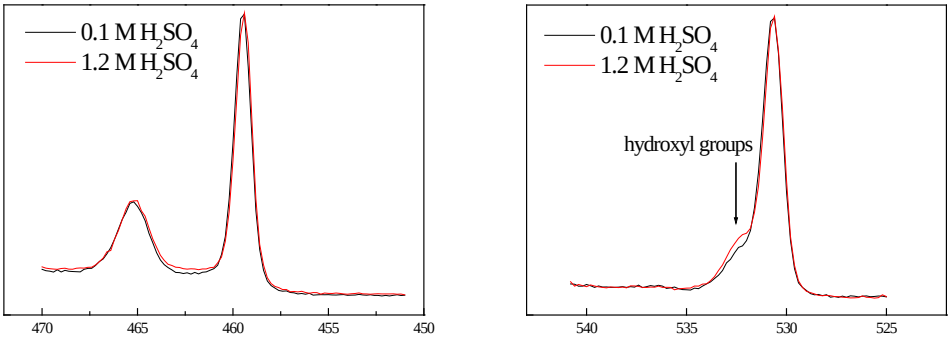

FIG. 6 Ti 2p (left) and O 1s (right) XPS spectrum of the oxides anodized in an electrolyte of a sulfuric acid concentration of 0.1 M and 1.2M.

3.4 Adhesion strength

Adhesion strength between the anodic oxide and the Ti substrate was characterized by the load-bearing capacity of the oxide layer using scratch test. Figure 7 shows the friction signal of the oxide anodized in an electrolyte of a sulfuric acid concentration of 0.1 M (a) and 1.2 M (b) with anatase TiO_2 prepared by sol-gel method (c) [10]. Distinct signal change (blue line) is found in (a) and (c), while continuous change is found in (b). The adhesion strength of the oxide anodized in an electrolyte of a sulfuric acid concentration of 0.02 M, 0.1 M, 0.2 M

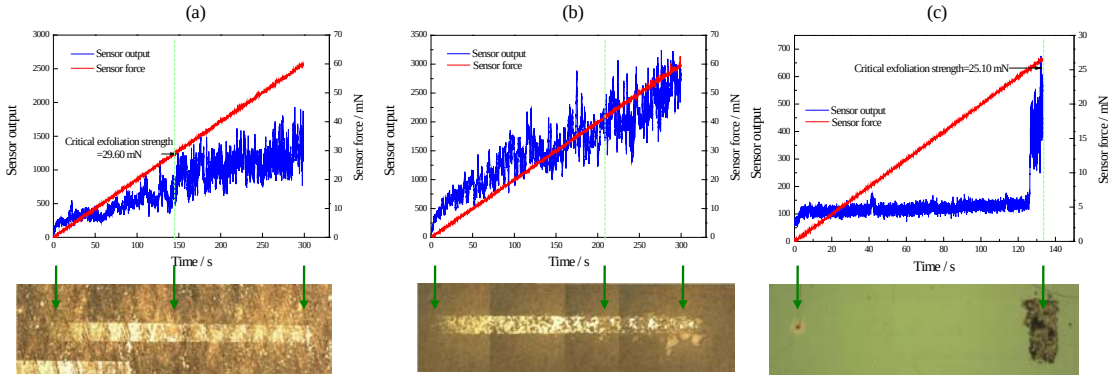

FIG.7 Friction signal (blue) in the scratch test of the oxide anodized in an electrolyte of a sulfuric acid of 0.1 M (a) and 1.2 M (b) with TiO_2 prepared by sol-gel method (c).

and 1.2 M are calculated as 26.60 mN, 28.63 mN, 32.10 mN and over the detection limit, respectively. On the other hand, those of the oxide prepared by sol-gel methods and CVD are 24.53 mN and 14.87 mN. This result suggests that the anodic oxide has high adhesion strength with an increase of sulfuric acid concentration in the electrolyte.

3.5 Photocatalytic activities

Figure 8 plots MB degradation calculated reaction rate constant under UV light illumination against concentration of sulfuric acid in the electrolyte [6]. The predominant oxide phase is replaced from anatase to rutile at 0.4 M of sulfuric acid concentration with an increase of sulfuric acid concentration, and the rutile form exhibits high MB degradation rate as compared to anatase form. In addition, an annealed oxide (red mark) is higher in the MB degradation rate than as-anodized oxide (blue mark) irrespective of the predominant phase.

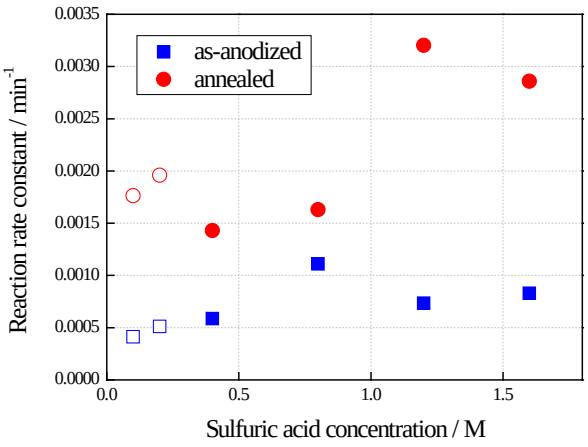

FIG. 8 Plots of MB degradation calculated reaction rate constant against the sulfuric acid concentration in the electrolyte.

Figure 9 shows the wavelength dependence of the photocatalytic activity of the anodic oxides and commercially available anatase oxide prepared by sol-gel method [7]. At longer wavelengths of visible light, the MB degradation rate of the anatase-structured anodic oxide prepared in 0.02 M and 0.1 M sulfuric acid aqueous solution was quite low, which is similar to the commercially available anatase-structured TiO_2. In contrast, the rutile-structured anodic oxides prepared in 1.2 M sulfuric acid aqueous solution exhibited photocatalytic activity when illuminated with visible light.

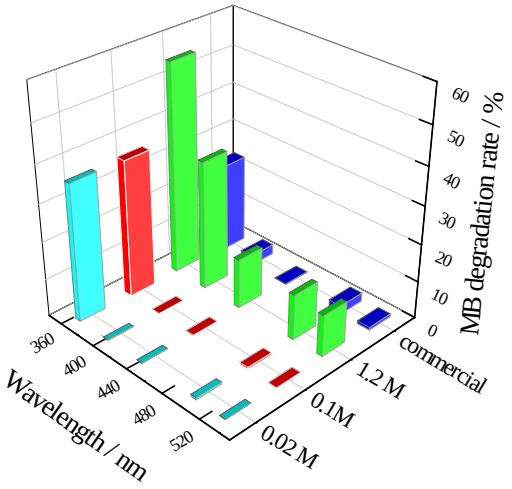

FIG.9 The wavelength dependence of MB degradation rate of the anodized TiO_2 in 0.02 M, 0.1 M, 1.2 M sulfuric acid and commercially available TiO_2.

Figure 10 summarizes the yield of CO_2 by acetaldehyde decomposition under visible light illumination with a wavelength longer than 400 nm and 422 nm for 1 h [10]. It is explicit that the oxide anodized in an electrolyte of a sulfuric acid concentration of 1.2 M records the highest yield irrespective of the wavelength of the illuminated light among the investigated samples.

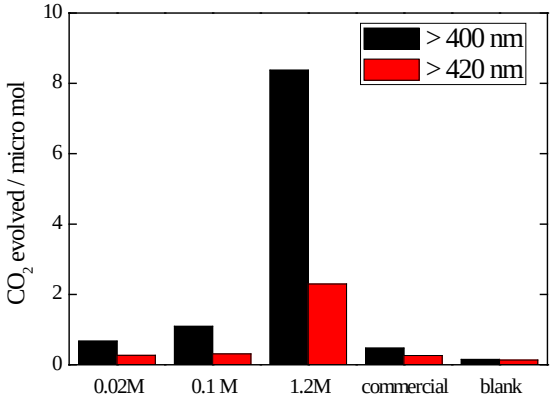

FIG.10 Yield of CO_2 in the photocatalytic decomposition of acetaldehyde under visible light illumination with a wavelength longer than 400 nm and 422 nm for 1 h.

3.6 Hydrophilicity

Figure 11 shows the plots of the contact angle against the duration of UV illumination for the anodic oxide; as-anodized (a) and annealed (b). The contact angle of the oxide prepared in an electrolyte with a high sulfuric acid concentration is lower than that in an electrolyte with a low sulfuric acid

concentration, regardless of the duration of UV light illumination before annealing. In the annealed anodic oxides, it should be noted that in the absence of UV light illumination, the contact angle of the oxide prepared in an electrolyte with a high sulfuric acid concentration is quite low.

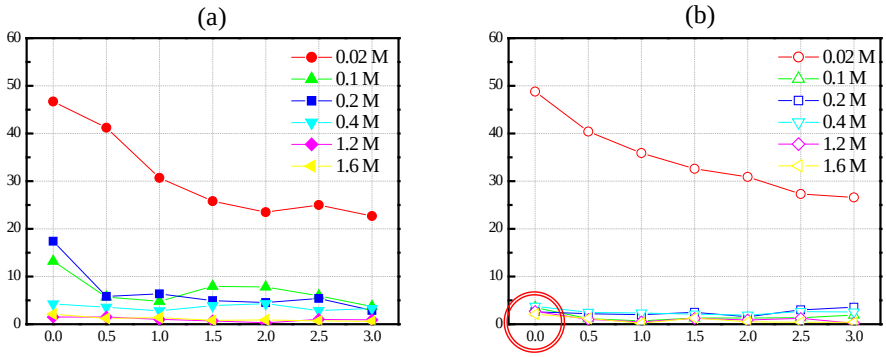

FIG.11 Plots of the contact angle against the duration of UV illumination for the oxide; as-anodized (a) and annealed (b).

Figure 12 shows the images of a water droplet with a drop size of 400-pL before (a) and 5 ms after (b) being dropped on the surface of the oxide prepared in 1.2M sulfuric acid [5]. The change in the volume of the water droplet is plotted against the elapsed time (c). The change in the volume of a 180-pL water droplet dropped on the surface of the oxide prepared in 0.1M sulfuric acid is used as the

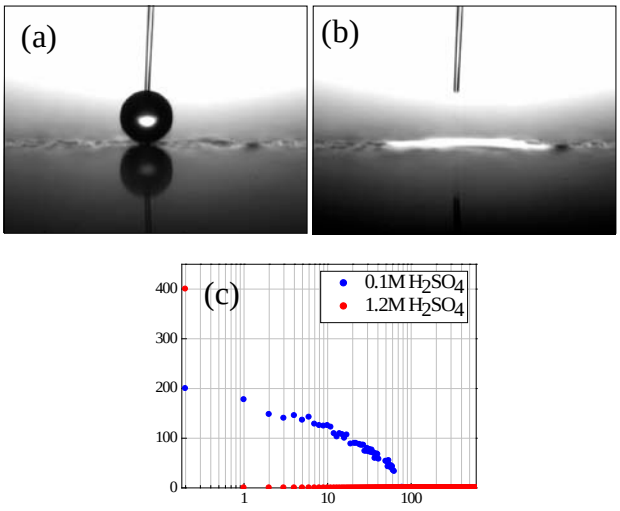

FIG.12 Images of the 400-pL water droplet before (a) and 5 ms after (b) being dropped on the surface of the oxide prepared in 1.2M sulfuric acid, and the change in the volume of the droplet against the elapsed time (c).

reference. The 400-pL water droplet is perfectly spread across the surface within 1 ms, and the water contact angle becomes zero. This is an extremely interesting phenomenon because the water droplet is spread across the surface at a rather high speed and it occurs in the absence of UV light illumination.

4. Consideration

4.1 Visible light response

The visible light response of TiO_2 photocatalyst is attributed to the electronic structure, and band gap narrowing is required to improve the property. The first principle calculation predicted a priority of anion ion doping such as nitrogen and sulfur [11], and the validity of nitrogen doping was reported [12-16]. Figure 13 illustrates the band gap structure of TiO_2 with doping [17]. The visible light response arises from occupied N 2p localized states located above the valence band edge with interstitial N 2p states lying further up from the valence band. The presence of localized states near the valence band edge has been said to be at the origin of the visible-light activity of anion-doped TiO_2. On the other hand, cation or defect-derived states at 2.0-2.5 eV above the valence band results in narrowing the band gap. However, this lower the oxidizing power and cation could be a recombination site. Therefore, the left side design in Figure 13 is recommended to achieve visible light response.

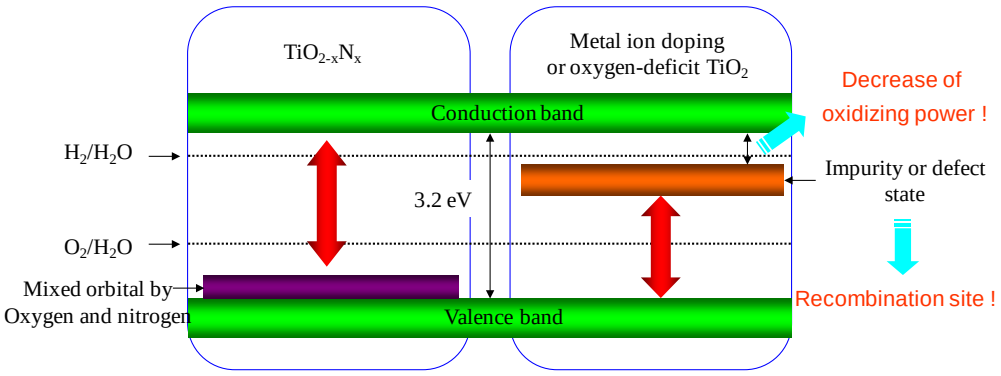

FIG. 13 Band gap structure of TiO_2 on doping it with nonmetals.

The present anodic oxide shows visible light response, and it is considered to be due to the modification of band gap structure by sulfur doping provided from the sulfuric acid in the electrolyte. Sulfur was detected from the anodic oxide by XPS analysis as shown in Figure 14(a), and sulfur existed over the oxide with

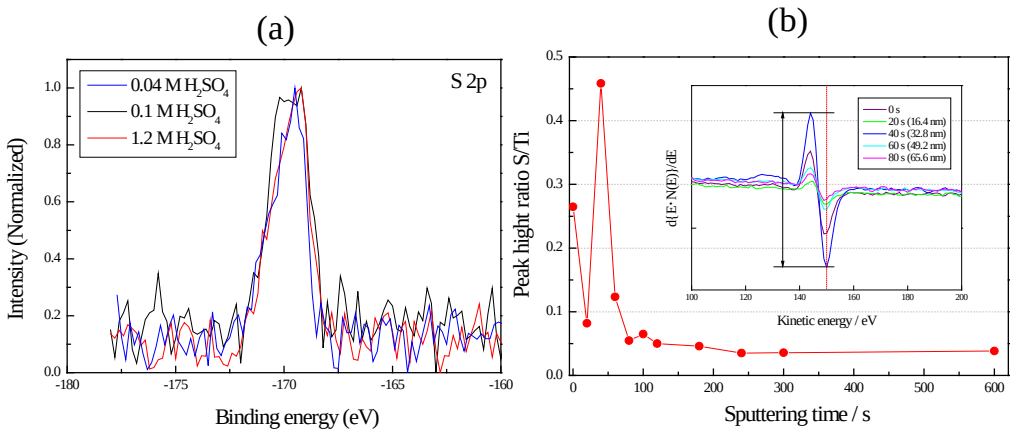

FIG.14 S 2p XPS of the anodized TiO_2 (a) and a plot of the peak height ratio of sulfur (152 eV) to titanium (418 eV) during sputtering for the oxide anodized in an electrolyte of 1.2 M sulfuric acid (b). (AES spectra of before and after sputtering for 20, 40, 60, and 80 s are inserted in (b))

segregation near the surface as shown in Figure 14(b). The amount of sulfur was analyzed by measuring SO_2 [7] extracted from the oxide during combustion in high frequency furnace, and the result is shown in Figure 15 [7]. Assuming that density of TiO_2 is 4.23 g/cm^3 and the thickness of the layer is fixed as the value determined by cross-section TEM observation, the sulfur concentration in the oxide could be calculated; 1.83 at.%, 1.50 at. %, 0.73 at. %, 0.38 at. %, 0.36 at. %, and 0.17 at. % for the oxides anodized in an electrolyte of a sulfuric acid concentration of 0.002 M, 0.02 M, 0.1 M, 0.2 M, 0.4 M and 1.2 M, respectively. Thus, the sulfur concentration in the oxide decreases with sulfuric acid concentration in the electrolyte.

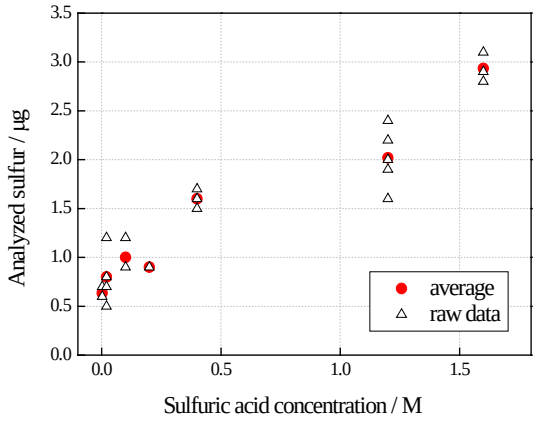

FIG. 15 Plots of the analyzed sulfur content against the sulfuric acid concentration in the electrolyte.

According to theoretical calculation[11], sulfur doping is difficult as compared with nitrogen doping, because large formation energies is required for sulfur doping to substitute sulfur for oxygen in TiO_2. Several studies to fabricate sulfur-doped photocatalytic oxide have been reported; oxidation of TiS2 powder [18], sol–gel techniques using thiourea [19] and ion-implantation [20]. Distinct difference between the present oxide and references is a form of TiO_2; the present oxide is rutile, whereas the reference oxide is anatase. Calculation of the electronic band structure focusing on crystal structure and site occupation of sulfur is in progress by using first-principle method.

4.2 Superhydrophilicity

The present results show that the contact angle of the oxide prepared in an electrolyte with a high sulfuric acid concentration is lower than that with a low sulfuric acid concentration and is quite low in the absence of UV light illumination. As revealed in Figure 6, the former anodic oxide could adsorb a large amount of water molecules as compared to the latter oxide. Figure 16 shows O 1s XPS spectra of the as-anodized (left) and annealed (right) oxides prepared in an electrolyte of 1.2 M sulfuric acid concentration for the following conditions: before illumination (a), exposure to oxygen (0.5 kPa) for 5 min under UV illumination (b), UV illumination for 30 min in the analysis chamber (c), and exposure to air (1.05 kPa) for 1 h followed by UV illumination in the analysis chamber (d) [4]. All the oxides show an asymmetric O 1s XPS due to the adsorption of water molecules, and the intensity of the shoulder peak in the

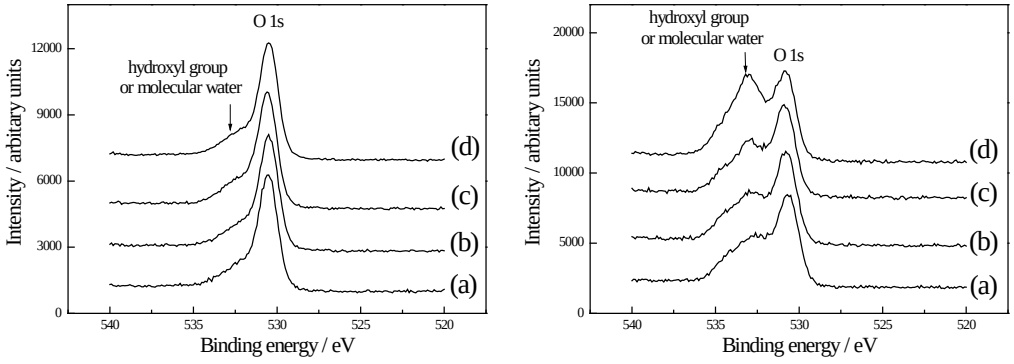

FIG. 16 O 1s XPS spectra of the as-anodized (left) and annealed (right) oxides: before illumination (a), exposure to oxygen (0.5 kPa) for 5 min under UV illumination (b), UV illumination for 30 min in the analysis chamber (c), and exposure to air (1.05 kPa) for 1 h followed by UV illumination in the analysis chamber (d).

annealed oxide is higher than that in the as-anodized oxide regardless of the exposure and UV illumination. No difference was observed with regard to the intensity of the shoulder peak among the O 1s XPS of the as-anodized oxide, while the spectrum of the annealed oxide varies upon exposure and UV illumination treatment. These results imply that the annealed oxide interacts strongly with the hydroxyl groups.

The mechanism of superhydrophilicity is proposed based on a newly formed oxygen defect by Sakai et al [21]. In this model, the oxygen defect is formed after the surface oxygen traps two holes generated by the photocatalysis reaction. Water molecule adsorbs on this oxygen defect, and the water droplet spreads on the surface of the oxide. In this model, oxygen defects are required for superhydrophilicity under UV illumination. According to this proposed model, holes should be generated under visible light illumination in the present oxide. However, a generation of oxygen vacancy was not verified in the anodic oxide from Ti 2p XPS as shown in Fig. 5, the symmetrical shape of the Ti 2p XPS spectrum suggests that reduced Ti^{3+} ions are not present in the oxides. Further studies to explain the results in the current study have been in progress.

5. Conclusions

The photo-induced characteristics and adhesion strength of TiO_2 prepared by anodic oxidation are investigated. With an increase of sulfuric acid concentration in the electrolyte, the predominant phase converts from anatase to rutile. The crystallite size of rutile is constant at approximately 30 nm, and the inhomogeneous lattice strain is quite small or close to zero. The surface area increases due to the appearance of nano-sized pores in the oxide with an increase in the concentration of sulfuric acid in the electrolyte. Adhesion strength of the anodic oxide from the substrate increased with an increase of sulfuric acid in the electrolyte, which is benefit for durability in application. The contact angles of rutile-structured TiO_2 anodized in an electrolyte with a high concentration of sulfuric acid is almost zero in the absence of UV light illumination. XPS analysis revealed that the oxide interacts strongly with the hydroxyl groups. The photocatalytic activity is improved with an increase in the concentration of sulfuric acid and rutile exhibits better characteristics as compared to anatase. Moreover, rutile-structured TiO_2 degraded MB aqueous solution and yielded CO_2 by decomposing acetaldehyde under visible light illumination, in which the wavelengths of the illuminated light is longer than those corresponding to the

band gap of monolithic rutile TiO_2. This is attributable to a modification of the band-gap structure of the oxide by sulfur doping.

Acknowledgements

The authors wish to thank Prof. Hanada, Prof. Oku, Prof. Suzuki, Dr. Semboshi from Tohoku Univ., Dr. Ohtsu from Kitami Institute of Technology, Prof. Saito from Waseda Univ. and Prof. Maeda, Prof. Nishimura and Dr. Okitsu from Osaka Prefecture Univ. for their valuable discussions and encouragement for the pursuance of this study. The authors wish to acknowledge Ms. Matsuda and Mr. Sugiyama from IMR, Tohoku Univ. for sample preparations, Dr. Ashino and Mr. Sakamoto from IMR, Tohoku Univ. for chemical analysis, Mr. Murakami from IMR, Tohoku Univ. for AES experiments, Mr. Yamane from Kitami Institute of Technology for XPS experiments, and Mr. Ozawa and Dr. Moroishi from Tig. Co. Ltd. This study was partly supported by a Grant-in-Aid for Scientific Research (A) (No.17206070) from the Ministry of Education, Culture, Sports, Science, and Technology, Japan.

References

[1] A. Fujishima, K. Honda, *Nature* **238** (1972) 37−38.
[2] G.S. Turchi, D.F. Ollis, *J. Catal,* **122** (1990) 178-192.
[3] R.W. Matthews, *Pure Appl. Chem.* **64** (1992) 1285-1290.
[4] N. Masahashi, S. Semboshi, N. Ohtsu, M. Oku, *Thin Solid Films* **516** (2008) 7488-7496.
[5] N. Masahashi, Y. Mizukoshi, S. Semboshi, N. Ohtsu, *Chem. Lett.* **38** (2008) 1126-1127.
[6] N. Masahashi, Y. Mizukoshi, S. Semboshi, N. Ohtsu, *Appl.Catal., B* **90** (2009) 255-261.
[7] Y. Mizukoshi, N. Ohtsu, S. Semboshi, N. Masahashi, *Appl.Catal., B* **91** (2009) 152-156.
[8] N. Ohtsu, N. Masahashi, Y. Mizukoshi, and K. Wagatsuma, *Langmuir* **25** (2009) 11586–11591
[9] W. Choi, A. Termin, M.R. Hoffmann, *J. Phys. Chem*. **98** (1994) 13669-13676.
[10] Y. Mizukoshi, N. Masahashi, *Collected Abstracts of the 2010 Spring Meeting of the Japan Inst. of Metals,* (2010) p.303.

[11] R. Asahi, T. Morikawa, T. Ohwaki, K. Aoki, Y. Taga, *Science* **293** (2001) 269−271.
[12] H. Irie, Y. Watanabe, K. Hashimoto, *J. Phys. Chem. B* **107** (2003) 5483-5486
[13] T. Ihara, M. Miyoshi, Y. Iriyama, O. Matsumoto, S. Sugihara, *Appl.Catal., B* **42** (2003) 403-409.
[14] O. Diwald, T.L. Thompson, T. Zubkov, E.G. Goralski, S.D. Walck, J.T. Yates, *J. Phys. Chem. B* **108** (2004) 6004-6008.
[15] S. Sakthivel, M. Janczarek, H. Kisch, *J. Phys. Chem. B* **108** (2004) 19384-19387.
[16] M. Mrowetz, W. Balcerski, A.J. Colussi, M.R. Hoffmann, *J. Phys. Chem. B* **108** (2004) 17269-17273.
[17] A. Fujishima, *Sci. & Technol. J.* Feb. (2004) 66-69.(in Japanese)
[18] T. Umebayashi, T. Yamaki, S. Tanaka, K. Asai, *Chem. Lett.* **32** (2003) 330-331.
[19] J.C. Yu, W.K. Ho, J.G. Yu, H. Yip, P.K. Wong, J.C. Zhao, *Environ. Sci. Technol.* **39** (2005) 1175-1179**.**
[20] T. Umebayashi, T. Yamaki, S. Yamamoto, A. Miyashita, S. Tanaka, T. Sumita, K. Asai, *J. Applied Physics* **93** (2003) 5156-5160.
[21] N. Sakai, A. Fujishima, T. Watanabe, K. Hashimoto, *J. Phys. Chem. B* **105** (2001) 3023-3026.

Remarks

Part of this study was achieved by collaboration research project with plural private companies, and several patents concerning the current results have been applied.

Contact to
Naoya Masahashi
Institute for Materials Research, Tohoku University
e-mail: masahasi@imr.tohoku.ac.jp

Yoshiteru Mizukoshi
Institute for Materials Research, Tohoku University
e-mail: mizukosi@imr.tohoku.ac.jp